REVISTA INTERDISCIPLINAR DE PESQUISA EM ENGENHARIA

CILAMCE 2016
XXXVII IBERIAN LATIN AMERICAN CONGRESS ON COMPUTATIONAL METHODS IN ENGINEERING
BRASÍLIA - DF - BRAZIL

A MODIFIED FLOW ORIENTATION SCHEME COUPLED WITH A ROBUST MPFA-DIAMOND FOR THE SOLUTION OF TWO-PHASE FLOW IN HIGHLY ANISOTROPIC PETROLEUM RESERVOIRS

M. R. A. Souza

marciosouza@cear.ufpb.br

Department of Renewable Energy Engineering, UFPB

BR 230, km 21 s/n, CEP: 58059-900, João Pessoa, PB, Brazil Address, Zip-Code, State, Province, Country

F. R. L. Contreras

ferlicapac@gmail.com

P. R. M. Lyra

prmlyra@padmec.org

D. K. E. Carvalho

dkarlo@uol.com.br

Department of Mechanical Engineering, UFPE

Av. Acadêmico Hélio Ramos s/n, CEP: 50670-901, Recife, PE, Brazil

Abstract. *In this paper we simulate two-phase flow in anisotropic petroleum reservoirs. The IMPES procedure is used to solve the coupling between pressure and saturation equations. The pressure equation is discretized by a robust Multipoint Flux Approximation Method with a Diamond-type support. This formulation is capable of reproducing piecewise linear solutions exactly and deals with anisotropic media. To solve the saturation equation a Modified Flow Oriented Scheme (M-FOS) is proposed. This alternative computes the multidimensional numerical fluxes using higher order accuracy in space. This formulation explicitly takes into account the angular distortion of the computational mesh by means of an adaptive weight that tunes the multidimensional character of the formulation according to the grid distortion. A recently devised Multidimensional Limiting Process is adopted in this paper*

to control the spurious oscillations in higher order approximation. This strategy guarantees monotone solutions and can be used with any polygonal mesh. Finally, an efficient entropy fix strategy, originally proposed in magneto-dynamics context, is also employed in order to produce convergent solutions. The performance of this set of numerical schemes is verified by solving some relevant benchmark problems, where we observe that the Grid Orientation Effects are clearly diminished by using this M-FOS framework.

Keywords: *Oil and Water displacements, Anisotropic Porous Media, MPFA-D, MLP, Modified Flow Oriented Scheme*

1 INTRODUCTION

Standard reservoir simulators employ, in general, Two-Point Flux Approximation (TPFA) and First Order Upwind Scheme (FOUS) to approximate, respectively, the diffusive and advective fluxes (Lamine and Edwards, 2010). As extensively discussed in literature, although TPFA present robustness for Cartesian grids and diagonal permeability tensor, this scheme suffers from serious numerical limitations when arbitrary mesh and/or permeability tensor are considered (Lamine and Edwards, 2010). This enforces stringent constraints for those simulators which depend on this type of approximation. Besides, FOUS computes, by construction, the control surface fluxes with one-dimensional nature, by using only data associated to the control volumes that share the evaluated surface.

Several flow oriented schemes have been presented in literature aiming to diminish this dependence (Tran *et al*., 2005; Hurtado *et al*., 2007; Lamine and Edwards, 2010; Kozdon *et al*., 2011). All these schemes are, in a certain way, based on the pioneer work of Schneider and Raw (1986) and Colella (1990), both proposed in fluid dynamics context, but with different strategies. These schemes are predominantly with first order of accuracy and are characterized by using the correct upwind direction, which improve significantly the results obtained for classical benchmark problems. In addition, some of these schemes, such as those presented by Tran *et al*., (2005), Hurtado *et al*. (2007) and Kozdon *et al*. (2011) require the solution of local algebraic systems for computing the numerical fluxes. On the other hand, the Lamine and Edwards (2010) proposal are characterized by explicitly calculating the multidimensional numerical flux on each control surface, such as done by Colella (1990). The first higher order flow oriented scheme was proposed by Tran *et al*. (2005) also for thermo-fluid dynamics context. Recently, Lamine and Edwards (2013) also proposed a higher order variant for the schemes previously discussed in Lamine and Edwards (2010).

In this paper, we combine several numerical procedures in order to obtain a robust framework capable of produce convergent approximated solutions, even for problems which consider adverse fluid and rock properties or highly distorted meshes in the computational discretization. In this context, we discretize the pressure equation by a non-orthodox Multipoint Flux Approximation Method with a Diamond-type support (MPFA-D). This numerical scheme was initially proposed by Gao and Wu (2010), for general diffusion problems, and was recently introduced by Contreras *et al*. (2016) in petroleum reservoir context. As discussed in these works, MPFA-D is very robust and capable of reproducing piecewise linear solutions exactly by using a linear preserving interpolation with explicit weights. This avoids the solution of locally defined systems of equations, as often seen in another traditional MPFA schemes.

To solve the transport equation, we propose an alternative flow oriented scheme. This scheme diminishes the Grid Orientation Effects (GOE), especially for orthogonal grids, even

though some lack of robustness can be observed for extremely distorted meshes. In this type of scheme, the numerical flux is computed in each control surface in a multidimensional way, by a convex combination of the water saturation values, following the approximate flow orientation throughout the computational domain. However, the majority of the schemes found in literature is only with first order of accuracy in space and demand the implicit solution of local conservation problems. For the Modified Flow Oriented Scheme (M-FOS) here proposed, the truly multidimensional numerical fluxes are explicitly computed using either first or higher order accuracy in space. For the proposed scheme, the robustness and the multidimensional character of the aforementioned M-FOS explicitly takes into account the angular distortion of the computational mesh by means of an adaptive weight. This procedure tunes the multidimensional character of the formulation according to the grid distortion and clearly diminishing GOE. The suppression of the spurious oscillations, typical from higher order schemes, is achieved by using the Multidimensional Limiting Process (MLP). This strategy was devised by Park *et al*. (2010) for solving general aerodynamics problems and employed, for the first time, in petroleum industry context by Souza *et al*. (2015). Formally, MLP guarantees monotone solutions and can be used with any polygonal mesh and arbitrary orders of approximation. Finally, in order to guarantee physically meaningful solutions, a robust entropy fix strategy proposed by Serna (2009), in a magneto-dynamics context, is employed. This produces convergent solutions even for the typical non-convex flux functions that are associated to the Buckley-Leverett model. The performance of the proposed full finite volume formulation is verified by solving some relevant benchmark problems.

2 MATHEMATICAL FORMULATION

The basic governing equation for the oil and water displacement in petroleum reservoirs is briefly described in the present section. Let $\Omega \subset \Re^2$ represents a computational domain over a time interval $[0,t]$. We assume, without loss of generality, some simplifying assumptions, such as immiscible and incompressible fluids, undeformable rock and the absence of thermal, dispersion and capillarity effects. The mass conservation equation is, therefore, written as follows:

$$\frac{\partial(\phi\rho_i S_i)}{\partial t} = -\nabla\cdot(\rho_i \vec{v}_i) + q_i, \quad i = o, w \tag{1}$$

where ϕ is the rock porosity, S_i and ρ_i are, respectively, the saturation and density of each phase *i*, with $i = w$ for water (wetting phase) and $i = o$ for oil (non-wetting phase). The injection or production wells (i.e. source or sink terms) are indicated by q_i and the phase velocity $\vec{v}_i$ is given by a generalized form of the Darcy's law:

$$\vec{v}_i = -\lambda_i \underset{\sim}{K}\vec{\nabla} p_i, \quad i = o, w \tag{2}$$

In Eq. (2), ρ_i and λ_i are the density and mobility of *i*th phase, respectively. The phase mobility is given as $\lambda_i = k_{ri}/\mu_i$, where μ_i and $k_{ri}(S_i)$ represent, respectively, the viscosity and the relative permeability of phase *i*. The tensor $\underset{\sim}{K}(\vec{x})$ represents the absolute rock permeability, which satisfies the ellipticity condition, in which, for a 2-D domain, requires that $K_{xx}K_{yy} \geq K_{xy}^2$.

An additional assumption ensures that the reservoir rock is fully saturated by oil and water. Hence we can write a volumetric constraint as follows:

$$S_o + S_w = 1 \tag{3}$$

We will use a segregated formulation in which the basic equations are obtained from the proper combination of the mass conservation equation and the Darcy's Law. By using Eqs. (1) to (3) and after some algebraic manipulation (Aziz and Settari, 1979), we can write the elliptic pressure equation, as:

$$\vec{\nabla} \cdot \vec{v} = Q \quad \text{with} \quad \vec{v} = -\lambda \underset{\sim}{K} \vec{\nabla} p \tag{4}$$

where $\vec{\nabla} p$ denotes the pressure gradient, $\lambda = \lambda_o + \lambda_w$ is the total mobility and $\vec{v} = \vec{v}_w + \vec{v}_o$ is total velocity. The total fluid injection or production specific rate is denoted by $Q = Q_w + Q_o$ with $Q_i = q_i / \rho_i$.

For obtaining the saturation equation, we combine again the Eqs. (1) to (3) and manipulate it, algebraically, in order to get:

$$\phi \frac{\partial S_w}{\partial t} = -\nabla \cdot \vec{F}(S_w) + Q_w \tag{5}$$

In Eq. (5), the flux function is defined, in absence of gravity and capillarity, by $\vec{F}(S_w) = f_w \vec{v}$ where $f_w = \lambda_w / \lambda$ is the fractional flow of water, which is a non-linear function of the water-phase saturation. Eq. (5) is a non-linear hyperbolic equation from which discontinuous profiles can evolve even from smooth initial solutions (Aziz and Settari, 1979).

The problem described by Eqs. (4) and (5) is only completely determined when we use an appropriate set of initial and boundary conditions. Typical boundary and initial conditions are given by (Aziz and Settari, 1979):

$$\begin{aligned} &p(\vec{x},t) = g_D \quad on \quad \Gamma_D \times [0,t]; \quad \vec{v} \cdot \vec{n} = g_N \quad on \quad \Gamma_N \times [0,t]; \\ &S_w(\vec{x},t) = \overline{S}_w \quad on \quad \Gamma_I \times [0,t]; \quad S_w(\vec{x},0) = \overline{S}_w^0 \quad on \quad \Omega \quad at \quad t = t_0 \end{aligned} \tag{6}$$

where the scalar functions g_D (prescribed pressures) and g_N (prescribed fluxes) are, respectively, defined in Γ_D (Dirichlet) and Γ_N (Neumann) boundaries, with $\Gamma = \Gamma_D \cup \Gamma_N$ and $\Gamma_D \cap \Gamma_N = \varnothing$. The set of injection wells are represented by Γ_I (internal boundaries), in which the water saturation $\overline{S}_w$ is prescribed. Finally, $\overline{S}_w^0$ is the water saturation distribution at the initial time t_0.

3 NUMERICAL FORMULATION

In this paper the coupling between the Eq. (4) and (5) is resolved by using the Implicit Pressure Explicit Saturation (IMPES) strategy. In this procedure, the mobilities are evaluated from the saturation field computed in the previous time level. This fact decouples the computation of the pressure equation from the saturation equation, allowing the saturation to be explicitly calculated, while the pressure computation is kept implicit (Aziz and Settari, 1979). Through the next sections the robust numerical formulation here employed to solve both pressure and saturation equations are briefly described.

3.1 Finite Volume Discretization of the Pressure Equation

The Multi-Point Flux Approximation with Diamond Support (MPFA-D) is described in this section. This scheme was originally proposed to solve diffusion type problems in heterogeneous and anisotropic media (Gao and Wu, 2010). As depicted in Fig. 1, in this numerical scheme the flux on each control volume surface, of the primal polygonal mesh, is explicitly expressed by two cell-centered unknowns ($\hat{L}$ and $\hat{R}$), defined on the control volumes sharing that face and two vertex unknowns (I and J) at the two face's endpoints. In order to turn the method into a pure cell-centered scheme, the vertex unknowns are treated as intermediate ones being rewritten as linear combinations of the cell-centered unknowns by using appropriate interpolations (Gao and Wu, 2010; Contreras *et al.*, 2016).

To obtain the finite volume discretization with MPFA-D scheme we suppose that the physical domain Ω with boundary Γ is partitioned into a finite number of control volumes (CVs) denoted by $\Omega_{\hat{V}}$. By integrating the pressure equation (4) over an arbitrary control volume and by applying the Gauss divergence theorem, it can be written as:

$$\int_{\Gamma_{\hat{V}}} \vec{v}\cdot\vec{n}\, d\Gamma_{\hat{V}} = \int_{\Omega_{\hat{V}}} Q\partial\Omega_{\hat{V}}, \quad \text{where} \quad \int_{\Gamma_{\hat{V}}} \vec{v}\cdot\vec{n}\,\partial\Gamma_{\hat{V}} \cong \sum_{IJ\in\Gamma_{\hat{V}}} \vec{v}_{IJ}\cdot\vec{N}_{IJ} \text{ and } \int_{\Omega_{\hat{V}}} Q\partial\Omega_{\hat{V}} \cong \bar{Q}_{\hat{V}}\Omega_{\hat{V}} \qquad (7)$$

where $\vec{n}$ denotes the unit outward normal vector to the control surface $\Gamma_{\hat{V}}$. In Fig. 1, we show two adjacent control volumes that share a generic face IJ with vertices *I* and *J*. The normal vector to this face is here represented by $\vec{N}_{IJ}$. Henceforth, we will admit that $\left|\vec{N}_{IJ}\right| = \left|\vec{d}_{IJ}\right|$, where $\left|\vec{d}_{IJ}\right|$ denotes the norm of the vector that represents the length of the face IJ (edge IJ in 2-D domain). The two triangles, $\Delta\hat{L}IJ$ and $\Delta\hat{R}JI$, defined by edge nodes *I* and *J* and by the centroids of the adjacent control volumes denoted by $\hat{L}$ (left CV) and $\hat{R}$ (right CV) form a stylized diamond path that justifies the name of the scheme.

The computation of the approximated pressure and velocities is obtained by using the scheme devised in Gao and Wu (2010). This method ensures that the pressure gradients are piecewise constant and the pressure field is piecewise linear over the triangles that form the diamond path such as shown in Fig. 1. To this purpose, the estimated flow rate calculated on the face IJ, that is shared by the left $(\hat{L})$ and the right $(\hat{R})$ control volumes, is defined by:

$$\vec{v}_{IJ}\cdot\vec{N}_{IJ} = \tau_{IJ}\left[\, p_{\hat{R}} - p_{\hat{L}} - \upsilon_{IJ}\left(p_J - p_I\right)\right] \qquad (8)$$

where the scalar transmissibility τ_{IJ} and the non-dimensional tangential parameter υ_{IJ} are defined, as function of physical and geometric parameters, by:

$$\tau_{IJ} = -\lambda_{IJ}\frac{K^{(n)}_{IJ_{\hat{L}}}K^{(n)}_{IJ_{\hat{R}}}}{K^{(n)}_{IJ_{\hat{L}}}h^{\hat{R}}_{IJ} + K^{(n)}_{IJ_{\hat{R}}}h^{\hat{L}}_{IJ}}\left|\vec{d}_{IJ}\right| \quad \text{and} \quad \upsilon_{IJ} = \frac{\vec{d}_{IJ}\cdot\vec{d}_{\hat{L}\hat{R}}}{\left|\vec{d}_{IJ}\right|^2} - \frac{1}{\left|\vec{d}_{IJ}\right|}\left(\frac{K^{(t)}_{IJ_{\hat{L}}}}{K^{(n)}_{IJ_{\hat{L}}}}h^{\hat{L}}_{IJ} + \frac{K^{(t)}_{IJ_{\hat{R}}}}{K^{(n)}_{IJ_{\hat{R}}}}h^{\hat{R}}_{IJ}\right) \qquad (9)$$

The presentation of the geometrical and physical parameters as well as details about its computation can be found in Gao and Wu (2010) and Contreras et al. (2016). In Equation (8) p_I, p_J, $p_{\hat{L}}$ and $p_{\hat{R}}$ are the pressures at the vertices of the triangles $\Delta\hat{L}IJ$ and $\Delta\hat{R}JI$ depicted on Fig. 1.

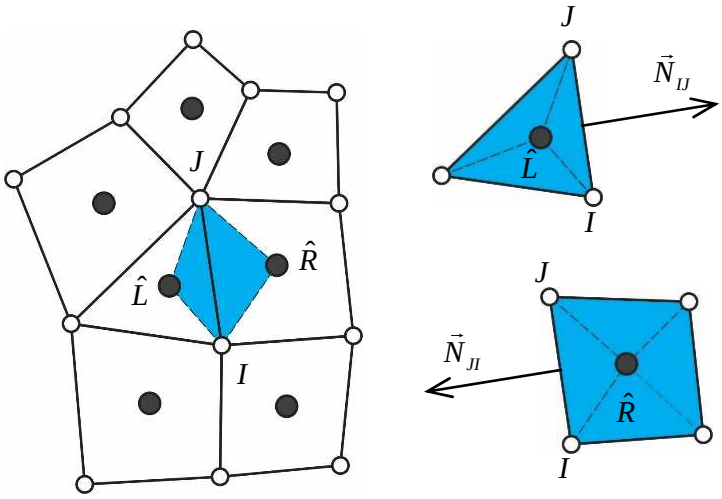

Figure 1. **Part of a polygonal mesh, illustrating the diamond path**.

For completeness, in Eq. (9) the mid-face mobility λ_{IJ} is obtained by using the volume average of the mobilities associated to the control volumes $\hat{L}$ and $\hat{R}$, that share the evaluated face. According Souza (2015) this interpolation strategy produces more accurate results when compared to other known strategies. The volume averaged mobilities are therefore given by:

$$\lambda_{w_{IJ}}\left(S_{w_{IJ}}\right), \qquad \text{where} \qquad S_{w_{IJ}} = \left(S_{w_{\hat{L}}}\Omega_{\hat{L}} + S_{w_{\hat{R}}}\Omega_{\hat{R}}\right) \Big/ \left(\Omega_{\hat{L}} + \Omega_{\hat{R}}\right) \tag{10}$$

In Eq. (10) $\Omega_{\hat{L}}$ and $\Omega_{\hat{R}}$ are the volumes (areas in 2-D domain) of the control volumes $\hat{L}$ and $\hat{R}$, respectively. The total mobilities $\lambda_{\hat{L}}$ and $\lambda_{\hat{R}}$ are therefore obtained from the water saturation $S_{w_{\hat{L}}}$ and $S_{w_{\hat{R}}}$, projected over the control volumes $\hat{L}$ and $\hat{R}$, respectively.

3.2 Finite Volume Discretization of the Saturation Equation

Again we take the computational domain Ω and discretize it in $\mathcal{N}_{VC}$ non-overlapping control volumes. We therefore integrate the saturation equation over an arbitrary control volume $\Omega_{\hat{V}}$ with surface $\Gamma_{\hat{V}}$ and through the time interval $[t_0, t_F]$, with t_0 and t_F denoting, respectively, the initial and final time. After applying the Gauss divergence theorem in the integral equation, the mean value theorem in the space term and first order forward Euler approximation in the time term, we obtain the discrete numerical equation for the solution of the non-linear hyperbolic saturation equation that can be written as:

$$S_w^{m+1} = S_w^m - \frac{\Delta t}{\phi \Omega_{\hat{V}}} \left(\sum_{IJ \in \Gamma_{\hat{V}}} \vec{F}_{IJ} \left(S_w^m \right) \cdot \vec{N}_{IJ} - \bar{Q}_w \Omega_{\hat{V}} \right) \tag{11}$$

where the superscripts *m* and *m+1* denote physical quantities existing at times t^m and t^{m+1}, respectively. The time step, denoted by Δt is defined as $\Delta t = t^{m+1} - t^m$ and must satisfy the CFL condition (Leveque, 2002). The source term $\bar{Q}_w$, which is non-zero only at wells, is here approximated by the mean value theorem (Contreras *et al*., 2016). The numerical flux on each surface IJ is here given as $\vec{F}_{IJ} \left(S_w^m \right) = f_w \left(S_w^m \right) \vec{v}_{IJ}$. Once the primary variable is usually not continuous through the control volume boundaries, we compute this numerical flux by using an approximated Riemann solver that guarantee a conservative flux and is given as:

$$\vec{F}_{IJ} \left(S_w^m \right) = \vec{\mathcal{F}}_{Riemann} \left(S_{w_{\hat{L}}}^m, S_{w_{\hat{R}}}^m \right) \tag{12}$$

For the standard first order approximation, $S_{w_{\hat{L}}}^m$ and $S_{w_{\hat{R}}}^m$ are the control volume projections on the left and right hand sides of each surface IJ evaluated. The standard second order approximation in space is achieved by replacing the arguments on Eq. (12) by extrapolated and suitably limited states, here denoted by $\tilde{S}_{w_{\hat{L}}}^m$ and $\tilde{S}_{w_{\hat{R}}}^m$. In this paper we also employ a flow oriented approach, with first and second order approximation in space. For those cases, the arguments on Eq. (12) are defined by upwind flow tracing on each half-surface evaluated. Additional details about the higher-order approximation, approximated Riemann solver and an entropy fix strategy are explained in Souza (2015).

Multidimensional Limiting Process. As an alternative to the traditional face-based limiter strategy, to be used in higher order schemes, we adopt a recently proposed Multidimensional Limiting Process (MLP). This control volume-based limiter was originally proposed by Park *et al*. (2010) for computing large scale aerodynamic problems and is based on the evaluation of extrema onto all vicinity surrounding the evaluated control volume. It produces a multidimensional feature for the limiter function. According to Park *et al*. (2010), MLP is able to effectively control spurious oscillations arising from multidimensional flows, especially when unstructured or distorted meshes are employed. MLP poses as a generalization of the traditional face-based limiters. This strategy can capture local flow details while other traditional control volume-based limiters smooth them.

To explain the basic idea of MLP strategy, let an arbitrary control volume $\hat{L}$ to be used as reference for computing the MLP limiter. This control volume is composed by a set of $\mathcal{N}_{vtx}$ vertices j, with $j = 1, ..., \mathcal{N}_{vtx}$. For each vertex j, $\mathcal{N}_M$ control volumes compose the vicinity $\hat{M}_i$, with $i = 1, 2, ..., \mathcal{N}_M$. The higher order numerical flux to be locally computed on the face *IJ*, must avoid extrema values in a multidimensional way, i.e., in all control volume vicinity, in order to ensure positive solutions for arbitrary configurations of flow orientation and mesh distortion. According to Park *et al*. (2010), extrema values always occur at the control volume vertices for linear approximations. Thus, the evaluation of extrema occurrence must be primarily evaluated for each vertex j. This must satisfy the following relationship:

$$S_{w,\min} \leq \tilde{S}_{w_j} \leq S_{w,\max} \tag{13}$$

where $S_{w,\min}$ and $S_{w,\max}$ denote, respectively, the maximum and minimum cell average values, among those associated to neighboring cells $\hat{M}_i$. In this case, the control volume $\hat{L}$ itself is also included in this evaluation.

The bound parameter $\tilde{S}_{w_j}$ in Eq. (13) denotes the second order water saturation, extrapolated up to the vertex j, following the MUSCL-type framework as:

$$\tilde{S}_{w_j} = S_{w_{\hat{L}}} + \vec{\nabla} S_{w_{\hat{L}}} \cdot \vec{d}_{\hat{L},j} \tag{14}$$

where $\vec{\nabla} S_{w_{\hat{L}}}$ is the water saturation gradient derived by means of *k*-exact polynomial reconstruction (Gooch, 1997) as aforementioned. The vector $\vec{d}_{\hat{L},j}$ represents the distance from the centroid of the control volume $\hat{L}$ to the vertex j. Based on the constraint presented in Eq. (13), the evaluation of extrema values for an arbitrary vertex j is therefore achieved by:

$$\mathcal{G}_{j,\hat{L}}^{MLP} = \begin{cases} \max\left[\min\left(1, \dfrac{S_{w,\max} - S_{w_{\hat{L}}}}{\tilde{S}_{w_j} - S_{w_{\hat{L}}}}\right), \min\left(1, \dfrac{S_{w,\min} - S_{w_{\hat{L}}}}{\tilde{S}_{w_j} - S_{w_{\hat{L}}}}\right)\right], & \text{if} \quad \tilde{S}_{w_j} - S_{w_{\hat{L}}} \neq 0 \\ 1, & \text{if} \quad \tilde{S}_{w_j} - S_{w_{\hat{L}}} = 0 \end{cases} \tag{15}$$

The parameter $\mathcal{G}_{j,\hat{L}}^{MLP}$ is bounded within the range [0,1] and denotes the MLP constraint for each vertex j which belongs to the control volume $\hat{L}$. Note that the ratios in Eq. (15) represent a comparison between the cell average values and the vertex extrapolated values. Both relative to the cell average value computed at the control volume $\hat{L}$. According to the main idea of MLP limiter, when the vertex value, relative to $S_{w_{\hat{L}}}$, is bigger than the maximum cell average value in vicinity cells $\hat{M}_i$, also relative to $S_{w_{\hat{L}}}$, the parameter $\mathcal{G}_{j,\hat{L}}^{MLP}$ must be lower than unity. An analogous relationship applies for the minimum cell average value. On the other hand, if the extrapolated value at the vertex is bounded by the maximum and minimum cell average values, $\mathcal{G}_{j,\hat{L}}^{MLP} = 1$ for any ratio bigger than 1. Thus, the MLP limiter is effectively defined $\forall j \in \hat{L}$ by:

$$\psi_{\hat{L}}^{MLP} = \min_{\forall j \in \hat{L}} \left(\mathcal{G}_{j,\hat{L}}^{MLP} \right) \tag{16}$$

The control volume-based limiter, defined by Eqs. (15) and (16), ensures that extrema values do not appear for any face IJ of the evaluated control volume $\hat{L}$. This gives the multidimensional character of the MLP limiter. Once the limiter is defined for all control volumes that discretize the domain, the higher order approximation for any face IJ in the computational mesh is achieved by:

$$\tilde{S}_{w_{IJ}} = S_{w_{\hat{L}}} + \psi_{\hat{L}}^{MLP} \vec{\nabla} S_{w_{\hat{L}}} \cdot \vec{d}_{\hat{L},\overline{c}} \tag{17}$$

where $\tilde{S}_{w_{IJ}}$ denotes the higher order approximation of water saturation on the face IJ. The vector $\vec{d}_{\hat{L},\overline{c}}$ represents the distance between the centroid of the control volume $\hat{L}$ and the mid-face point $\overline{c}$ (quadrature point) on the face IJ.

Alternatively, by using the Venkatakrishnan modification for the Barth-Jespersen limiter (Venkatakrishnan, 1995), Park *et al*. (2010) also devise a variant for the MLP limiter. In this proposal the limiter function is smooth and hence differentiable, which does not occurs for the function presented in Eq. (16). Thus, following an analog strategy presented in Eqs. (15) and (16), we have for each vertex j the following constraint:

$$\mathcal{G}_{j,\hat{L}}^{MLPvk} = \frac{\varpi^2 + 2\varpi + \varepsilon}{\varpi^2 + \varpi + 2 + \varepsilon}, \quad \text{with} \quad \varpi = \frac{\Delta_{CV}}{\Delta_{vtx}} \tag{18}$$

where Δ_{vtx} denotes the difference $\tilde{S}_{w_j} - S_{w_{\hat{L}}}$, involving the vertex value, $\forall j \in \hat{L}$. Such as observed in Eq. (16), Δ_{CV} also denotes a relationship taking in account either the maximum or the minimum cell average values, defined by:

$$\Delta_{CV} = \begin{cases} S_{w,\max} - S_{w_{\hat{L}}}, & \text{if} \quad \tilde{S}_{w_j} - S_{w_{\hat{L}}} > 0 \\ S_{w,\min} - S_{w_{\hat{L}}}, & \text{if} \quad \tilde{S}_{w_j} - S_{w_{\hat{L}}} < 0 \end{cases} \tag{19}$$

The parameter ε in Eq. (18) must be a quite small number (Park and Kim, 2012). Such as done in Eq. (16), once again the control volume-based limiter, MLPvk, is obtained for the control volume $\hat{L}$ by:

$$\psi_{\hat{L}}^{MLPvk} = \min_{\forall j \in \hat{L}} \left(\mathcal{G}_{j,\hat{L}}^{MLPvk} \right) \tag{20}$$

In the section devoted to numerical experiments the limiters MLP, MLPvk and the traditional van Albada are compared for some classical benchmark problems.

Approximated Riemann Solvers and Entropy Fix. Conventionally the Roe flux has been predominantly employed, even for simulation of flow in petroleum reservoir (Lamine and Edwards, 2010). Alternatively, the Local Lax Friedrichs (LLF) can be used for calculating the numerical flux on the face IJ. This type of approximation, in general, ensures entropy satisfying. However, it is well-known that LLF produces more diffusive numerical solutions than that obtained by the Roe approximation (Leveque, 2002). Serna (2009) proposes for magneto-dynamics application a variant of Shu and Osher (1989) entropy fix. In this novel strategy the LLF flux is used when either the sonic point or the so-called phase point occur. The phase point occurs when the states on the left and on the right are in different sides of the function which represents the derivative of fractional flux. Thus, the evaluation of the second derivative of the fractional flux is an indicator of the phase point existence. Serna (2009) criterion is therefore given as follows:

$$\vec{\mathcal{F}}_{Riemann}\left(S_{w_{\hat{L}}}^{m}, S_{w_{\hat{R}}}^{m}\right)\cdot\vec{N}_{IJ}=\begin{cases}\vec{\mathcal{F}}_{w_{IJ}}^{LLF}\cdot\vec{N}_{IJ}, & \text{if} \quad \left\{\dfrac{\partial f_w}{\partial S_w}\cdot\dfrac{\partial f_w}{\partial S_w}<0 \ \text{ or } \ \dfrac{\partial^2 f_w}{\partial S_w^2}\cdot\dfrac{\partial^2 f_w}{\partial S_w^2}<0\right. \\ \vec{\mathcal{F}}_{w_{IJ}}^{Roe}\cdot\vec{N}_{IJ}, & \text{otherwise}\end{cases} \tag{21}$$

In both approximated Riemann solvers, higher order approximation can be achieved by replacing the first order argument S_w by an extrapolated and suitably limited $\tilde{S}_w$ value, for both states on the left and on the right.

3.3 Modified Flow Oriented Scheme

In this section we introduce an alternative way to compute the Flow Oriented Schemes such as that applied by Hurtado *et al*. (2007) for the petroleum industry context. First and higher orders of approximation are presented for this alternative procedure. Other higher order flow oriented schemes are presented in Tran *et al*. (2005) and Lamine and Edwards (2013). Thus, considering the mesh fragment shown in Fig. 2, we introduce $\bar{n}(J)$ which represents the set of all half-surfaces belonging to the interaction region evaluated. Analogously, $\hat{c}(J)$ represents the set of control volumes sharing the vertex J as shown in Fig. 2. The number of half-surfaces in the interaction region is here denoted by $\mathcal{N}_{HS}$ and $\mathcal{N}_{CV}$ is the number of control volumes surrounding J.

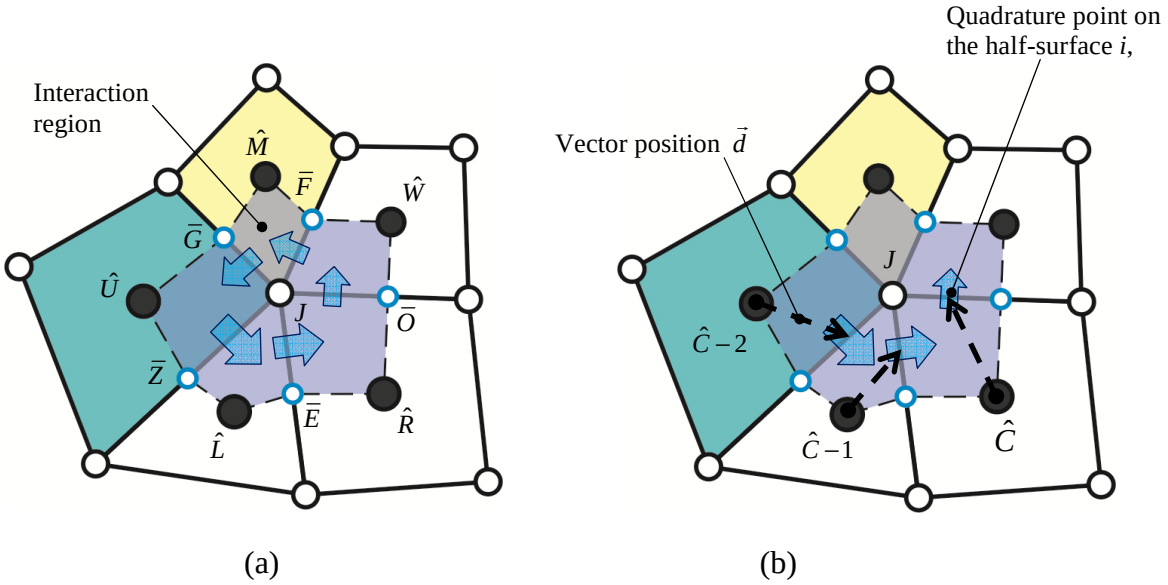

Figure 2. Interaction region for node *J* with the flow rate distribution through the half-faces: (a) velocities in counter clockwise only; (b) indication of the evaluated half-surface *i*, where a higher order value is calculated, and the vector position $\vec{d}$ used in extrapolation from the control volumes $\hat{C}$, $\hat{C}-1$ and $\hat{C}-2$.

Taking a general half-surface $\bar{E}J$ depicted in Fig. 2a, we can approximate the numerical flux through that by:

$$\vec{\mathcal{F}}_{\bar{E}J}\cdot\vec{N}_{\bar{E}J}=\breve{f}_{w_{\bar{E}J}}\vec{v}_{\bar{E}J}\cdot\vec{N}_{\bar{E}J} \tag{22}$$

where $\vec{\mathcal{F}}_{\bar{E}J}$ and $\vec{v}_{\bar{E}J}$ are, respectively, the numerical flux and the total velocity calculated over the evaluated half-surface $\bar{E}J$. The vector $\vec{N}_{\bar{E}J}$ is the outward normal vector and represents the area of the evaluated half-surface. The fractional flux $\breve{f}_{w_{\bar{E}J}}$ is here defined on the quadrature point of the evaluated half-surface. By considering the case shown in Fig. 2b, where all half-surfaces in $\bar{n}(J)$ are upstream concerning to the half-surface $\bar{E}J$, for example. For this case we can write $\breve{S}_{w_{\bar{E}J}}$ in an explicit way, i.e., free of solving the local algebraic system. This simply can be done by combining all equations established for the half-surfaces in $\bar{n}(J)$. After some algebraic manipulations, the multidimensional variable $\breve{S}_{w_{\bar{E}J}}$ can be written in a general way as:

$$\breve{S}_{w_i} = \frac{1}{\left(1-\prod_{j=1}^{\mathcal{N}_{HS}} w_j\right)}\left[\left(1-w_i\right)S_{w_{\hat{C}}} + \sum_{k=1}^{max\left(1,\mathcal{N}_{UHS}^{i}\right)}\left(\prod_{m=0}^{k-1} w_{i-m}\right)\left(1-w_{i-k}\right)S_{w_{\hat{C}-k}}\right] \tag{23}$$

where the evaluated half-surface is denoted by i. Those upstream half-surfaces are, respectively, denoted by $i-1$, $i-2$, …, $\mathcal{N}_{UHS}^{i}$. Analogously, the upstream control volume index are here denoted by $\hat{C}$, $\hat{C}-1$, $\hat{C}-2$, …, $\mathcal{N}_{UCV}^{i}$ as pointed in Fig. 2b. We enforce that $\mathcal{N}_{UHS}^{i} = \mathcal{N}_{HS} - 1$ and $\mathcal{N}_{UCV}^{i} = \mathcal{N}_{CV}$. Further details concerning to Eq. (23) derivation, can be found in Souza (2015). The amount of upstream half-surfaces, $\mathcal{N}_{UHS}^{i}$, taken into account defines each particular case. Since $\breve{S}_w$ is calculated on the $\mathcal{N}_{HS}$ half-surfaces, the flow oriented fractional flux on these half-surfaces can be obtained as $\breve{f}_w = \breve{f}_w\left(\breve{S}_w\right)$.

Finally, the weight $w_{\bar{E}J}$, for the half-surface $\bar{E}J$ is parameter which vary between 0 and 1, defined for each evaluated half-surface according to a local adaptive procedure, i.e., there exist a weight w for each half-surface belonging to $\bar{n}(J)$. Different strategies can be employed to derivate w as will be discussed in the next section. For all of them, $w=0$ when an evaluated half-surface does not have an upstream half-surface. In this case, the traditional one-dimensional upwind approximation is recovered and $\breve{S}_{w_{\bar{E}J}} = S_{w_{\hat{L}}}$. For $w \neq 0$, $\breve{S}_{w_{\bar{E}J}}$ is written as a linear convex combination between a known variable $S_{w_{\hat{L}}}$ and an unknown variable $\breve{S}_{w_{\bar{E}J}}$. Those variables are the water saturation associated, respectively, to the upstream control volume ($\hat{L}$) and to the quadrature point on the upstream half-surface ($\bar{E}J$).

The explicit higher order M-FOS approximation works in accordance with the idea previous developed for the first order approximation. In Fig. 2b we can see that the water saturation taken into account on the half-surface *i* is obtained by a MUSCL-type extrapolation procedure. In this paper Eq. (17) is employed. Both limiter MLP or MLPvk can be used. The control volume $\hat{C}$ is assumed as upstream according to the flow orientation such as done by Tran *et al*. (2005) in an implicit approach, i.e., solving local algebraic systems. In the present

paper the reconstructed variable over a certain half-surface is conveniently denoted by $\tilde{S}_{w_{\hat{C}}}$, where the upper tilde means higher order approach.

3.4 Strategies for Calculating the Flow Oriented Weights

The linear convex combination presented in Eq. (23), regarding to the half-surface $\bar{E}J$, for instance, defines the upwind flow tracing in the sub-region of the evaluated interaction region. The linear interpolation makes the variable ranged from $S_{w_{\hat{L}}}$ to $\breve{S}_{w_{\bar{Z}J}}$, according to the value of the interpolant $w_{\bar{E}J}$. This interpolant must vary between 0 and 1 in order to guarantee a convex combination. Thus, for the flow multidimensionality to be took into account, the interpolant is often defined as a function of the local flowrate ratio $\Lambda_{\bar{E}J}$, presented as follows (Schneider and Raw, 1986):

$$\Lambda_{\bar{E}J} = \frac{\vec{v}_{\bar{Z}J} \cdot \vec{N}_{\bar{Z}J}}{\vec{v}_{\bar{E}J} \cdot \vec{N}_{\bar{E}J}} \tag{24}$$

Since the ratio presented in Eq. (24) can be eventually bigger than 1, some here called control functions have been used in literature for maintaining $w_{\bar{E}J}$ bounded in the aforementioned range. In the pioneer strategy proposed by Schneider and Raw (1986), the control function poses as a natural idea and has been still used in recent flow oriented strategies (Hurtado *et al.*, 2007; Lamine and Edwards, 2010; Kozdon *et al.*, 2011). Following the Kozdon *et al.* (2011) nomenclature, this control function is here called Tight Multidimensional Upstream (TMU) and is given, for the half-surface $\bar{E}J$ by:

$$w_{\bar{E}J}^{TMU} = \min\left(1, \Lambda_{\bar{E}J}\right) \tag{25}$$

Note that for this control function, any ratio $\Lambda_{\bar{E}J}$ bigger than 1 implies in a same value for $w_{\bar{E}J}^{TMU}$, i.e., $w_{\bar{E}J}^{TMU} = 1$ for $\Lambda_{\bar{E}J} > 1$, such as we can see in the graph depicted in Fig. 3a.

Alternatively, Hurtado *et al.* (2007) propose a continuous and smooth control function, named, in Kozdon *et al.* (2011), Smooth Multidimensional Upstream (SMU). Again, for the half-surface $\bar{E}J$, depicted in Fig. 3a, this alternative proposal is given by:

$$w_{\bar{E}J}^{SMU} = \frac{\Lambda_{\bar{E}J}}{1 + \Lambda_{\bar{E}J}} \tag{26}$$

This proposal ensures that for any ratio $\Lambda_{\bar{E}J}$, for example, we have a smooth and corresponding variation for $w_{\bar{E}J}^{SMU}$. In this case, the values of $\Lambda_{\bar{E}J}$ that tend to infinite, lead to an interpolant $w_{\bar{E}J}^{SMU}$ tending to unity (Hurtado *et al.*, 2007). According to Kozdon *et al.* (2011) the reduction of GOE for some benchmark problems are strongly influenced by choosing the type of control function. These authors highlighted that the SMU proposal produces much enhanced results for their test cases. On the other hand, Souza (2015) shows that the good performance of the SMU control function, face the TMU control function, is not an invariant. The type of mobility interpolation, in pressure-saturation equation coupling, can change this scenario and produces better results for using the TMU control function.

The main idea of these new control functions is to increase the multidimensionality for either TMU or SMU strategies whenever the angle between the evaluated half-surface ($\bar{E}J$ in Fig. 4a) and the upstream half-surface ($\bar{Z}J$ in Fig. 4a) is lower than 90°.

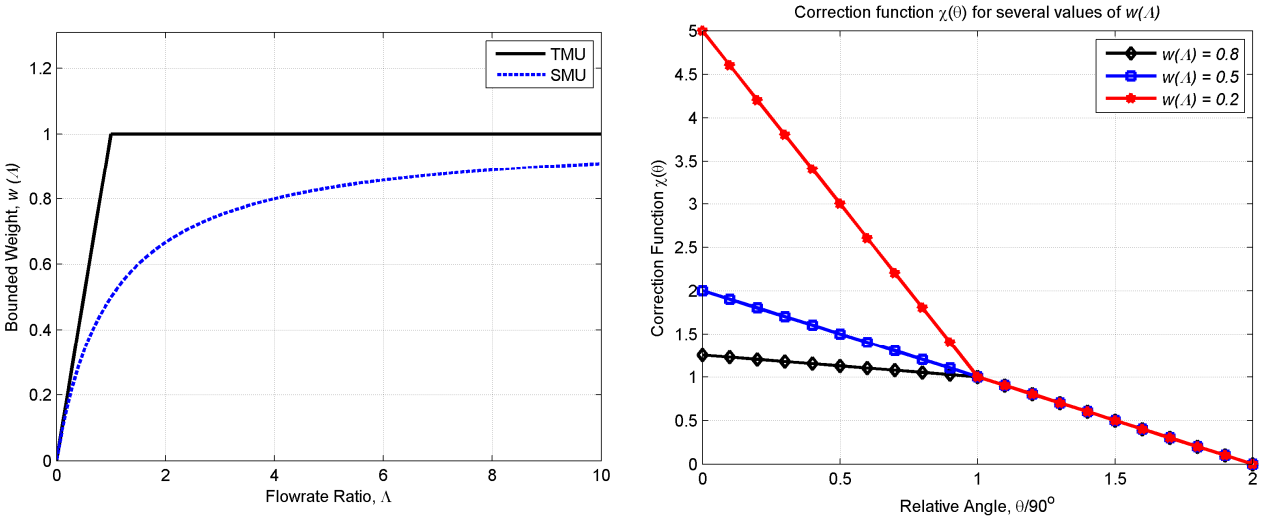

(a) (b)

Figure 3. Graphs employed for calculate the multidimensional weight for the Modified Flow Orientation Schemes: (a) representing both TMU and SMU control functions; (b) representing the correction function for different values of weight *w*.

On the other hand, when this angle is bigger than 90°, as shown in Fig. 4c, the multidimensionality must diminishes. Of course for meshes without distortion, both M-TMU and M-SMU return, respectively, to the traditional TMU and SMU control function. These modifications occur by modeling a correction function in order to produce the following relationship:

$$w^{M-TMU} = \chi(\theta)\, w^{TMU}; \qquad w^{M-SMU} = \chi(\theta)\, w^{SMU} \tag{27}$$

where $\chi(\theta)$ is modeled by imposing certain constraints. Initially we assume that $\chi(\theta)=1$ when $\theta=90^{\circ}$, where nothing changes. In addition, for an extreme acute angle, when $\theta=0^{\circ}$, we would have the maximum value of χ, where $\chi(\theta)=1/w$. On the other hand, for an extreme obtuse angle, when $\theta=180^{\circ}$, we would have the minimum value of χ, where $\chi(\theta)=0$. Thus we have the correction function $\chi(\theta)$ given by:

$$\chi(\theta)=\frac{1}{w}+\left(1-\frac{1}{w}\right)\frac{\theta}{90}, \quad \text{if} \quad \frac{\theta}{90}\le 1 \quad \text{or} \quad \chi(\theta)=2-\frac{\theta}{90}, \quad \text{if} \quad \frac{\theta}{90}>1 \tag{28}$$

Note that in Eq. (28), w can be either w^{TMU} or w^{SMU}, depending on the approach. In addition, we can obtain, at most, $w^{M-TMU}=1$ when $\chi(\theta)=1/w^{TMU}$, for $\theta=0^{\circ}$. At last, when $w=0$, Eq. (28) is not necessary since we have a traditional unidimensional approximation. In Fig. 3b the graph representing the function $\chi(\theta)$ is shown, for several values of w, as a

function of the relative angle $\theta/90$. We remark that this correction function is adaptive once w^{TMU} or w^{SMU} change with the flowrate ratio Λ, computed on each half-surface.

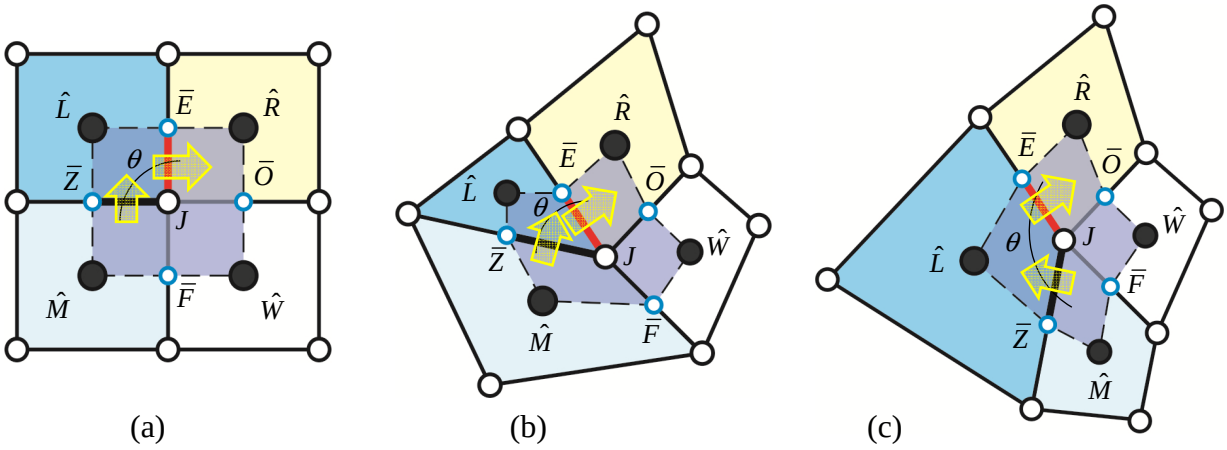

Figure 6. Multidimensionality correction according to the mesh distortion: (a) there is no influence of the mesh distortion, $\theta = 90^{\circ}$, $\chi(\theta) = 1$; (b) the control volume $\hat{L}$ is more upstream from the half-surface $\bar{E}J$, $\theta < 90^{\circ}$, $\chi(\theta) > 1$; (c) the control volume $\hat{L}$ is less upstream from the half-surface $\bar{E}J$, $\theta > 90^{\circ}$, $\chi(\theta) < 1$.

Finally, to perform these modifications, we proceed as follows:

1. Calculate the unmodified TMU or SMU control function by using, respectively, Eqs. (25) and (26);
2. For each half-surface, calculate the angle θ between the evaluated and the upstream half-surface (see Fig. 4);
3. Calculate a correction factor $\chi(\theta)$ by mean of Eq. (28);
4. Calculate the modified control functions M-TMU or M-SMU by using Eq. (27).

4 NUMERICAL RESULTS

Now we present some test cases in order to illustrate the benefits of the strategies proposed in this paper. Thus, we can observe how the higher order flow oriented scheme, associated to a multidimensional limiter strategy, correction procedure for distorted meshes and entropy fix can produce more reliable results when compared with that produced by another numerical schemes available in literature.

4.1. Buckley-Leverett Problem

In this test case, the Buckley-Leverett model, obtained from Bastian (2002), is numerically resolved employing schemes with both first and second order of accuracy in space. The simplified shape of the petroleum reservoir consists in an isotropic and homogeneous domain with constant porosity $\phi = 0.2$ and dimensions, given in meters, of [0,300]x[0,75]. The time interval consists in [0,1500] days. The permeability tensor is given by $\underset{\sim}{K} = \underset{\sim}{I}$. Known flow rate and water saturation are prescribed on the left face in the computational domain. This denotes the water injection in a rock initially saturated by oil.

The velocity of injection in that face is $v_w = 3\times10^{-7}$ m/s with unitary water saturation. Null Neumann flux is prescribed on both top and bottom surfaces, representing sealing faces. On the right face, we impose a known and null pressure. As adopted in Bastian (2002), the irredutible water saturation and residual oil saturation are, respectively, $S_{wi} = S_{or} = 0$. The mobility ration for this problem is $M = 1$ and the Brooks-Corey model is employed as constitutive relationship such as described in Bastian (2002). We also adopt the Courant number $\mathcal{C} = 0,5$. The computational domain is discretized with $\mathcal{N}_{CV} \times 1$ quadrilateral control volumes, where $\mathcal{N}_{CV}$ assumes 32, 64, …, 1024 subdivisions through the longitudinal direction. In order to evaluate the errors for the numerical solution, which are compared to the semi-analytical Welge solution (Aziz and Settari, 1979), the L_1 norm (Souza, 2015) is applied. In both cases, the solution is calculated on the colocation point with coordinate $\vec{x}$ through the computational domain. The parameter Ω_i denotes the volume (area in 2-D domain) of each control volume *i* where the solution is evaluated.

This test case aims to show that the convergence of the numerical solution towards the semi-analytical solution is strongly influenced by the use of the entropy fix strategy devised by Serna (2009). This fact is specially observed for higher order approximation results. We also evaluate here the different types of limitation strategies, for higher order approximation schemes, and their performance regarding to producing convergente solutions. In Fig. 5a we present the errors obtained with L_1 norm for the numerical solution of the Buckley-Leverett problem by using several mesh refinements.

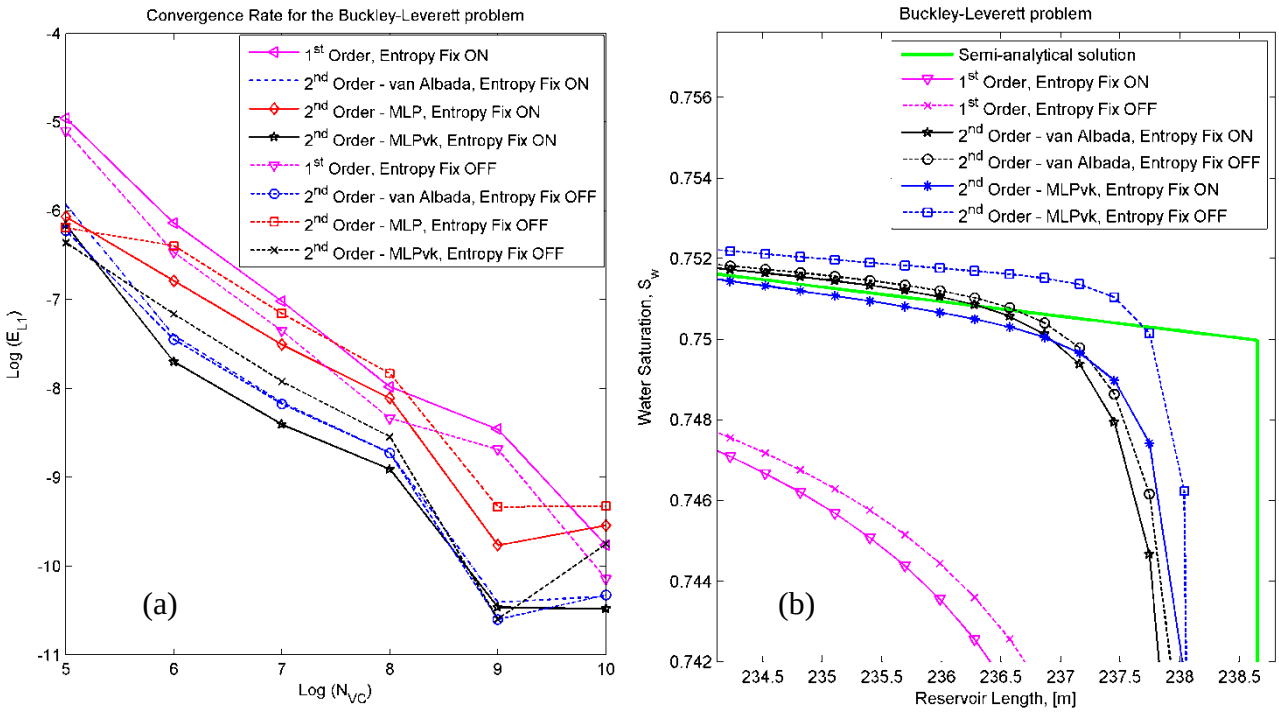

Figure 5. Buckley-Leverett problem: (a) convergence rate curves where solutions with and without entropy fix, obtained with first and second order of accuracy are compared; (b) zoom view of numerical results obtained in a mesh with 1024 subdivisions for first and second order of accuracy. Face-based limiter and the control volume-based limiters are also compared.

The traditional scheme with first order in space is therefore compared with that obtained with second order of accuracy and different limitations strategy (van Albada, MLP and MLP-vk). For all cases, numerical solutions with and without entropy fix are verified. Even though the effective convergence rate expected for each order of approximation cannot be reached due to the discontinuity in the solution, these results are an indicator of effectiveness for each numerical scheme. As shown in Fig. 5a, the convergence only occurs for the results obtained with first order approximation and second order with MLPvk limiter. The latter converges only when the entropy fix is employed (black continuous line). All other numerical schemes have the convergence degenerated for very refined meshes (1024 subdivisions). In this problem we obtain convergent solutions with the first order scheme, even when the entropy fix is not turned on. However, according Serna (2009), the absence of an entropy fix strategy can produce non-convergent solutions even for approximations with first order of accuracy. On the other hand, as aforementioned, the Serna (2009) strategy is strictly necessary for the convergence of second order approximation, even for a simpler test case. Besides, as shown in Fig. 5a, the results obtained exclusively with the Roe flux, i.e., without entropy fix (dashed lines) are, in general, worse than those obtained with entropy fix (continuous line). In Fig. 5b details of the numerical solutions are presented for a mesh with 1024 subdivisions. Note that, in a general way, only the first order approximation and the second order scheme, with MLPvk limiter and entropy fix, honored the semi-analytical solution such as previously indicated in the convergence analysis. In addition, the second order approximation limited with traditional face-based limiter produces non-physical solutions, even when the entropy fix is considered. This degrades the convergence rate as shown in Fig. 5a (blue lines).

4.2. Two-Phase Flow in Homogeneous and Anisotropic Petroleum Reservoir

The present test case consists of an adaptation from Lamine and Edwards (2010) problem. We consider here a homogeneous and anisotropic petroleum reservoir for a classical problem with a quarter of five-spot. The simplified petroleum reservoir has dimensions given by $[0,1]^2$. The permeability tensor presents anisotropy ratio $K_{xx}/K_{yy}=10$ and its main directions are rotated by 45° regarding to the Cartesian directions. This leads to a full-tensor for representing the permeability in Cartesian basis. Only null Neumann boundary condition is imposed through the boundary domain. Unitary flow rate and water saturation are prescribed on the injector well. On the producer well we have a known null pressure. For this problem we employ an adverse mobility ratio $M=50$. Irredutible water saturation S_{wi} and residual oil saturation S_{or} are both null. Again we adopt the Brooks-Corey model as the constitutive relationship. The exponents for the wetting and non-wetting phases are, respectively, $n_w=5$ and $n_o=1$. We also consider a final time for the simulation of 0.4 PVI and $C=0,5$. In this test case we intend to evaluate the performance of the modified flow oriented scheme, especially for second order of accuracy. We also evaluate the benefits of the procedure here proposed which adaptively tunes the multidimensionality of the flow oriented scheme according to degree of distortion in the meshes employed. For this test we employ a strongly distorted mesh, adapted from Hermeline (2007), with 32x32 and 64x64 subdivisions, shown in Fig. 6a and 6b, respectively. A reference solution was obtained with the robust schemes MPFA-O and First Order Upwind Scheme solving, respectively, the pressure and the saturation equations. An unstructured triangular mesh with 37,996 control volumes was used for this case.

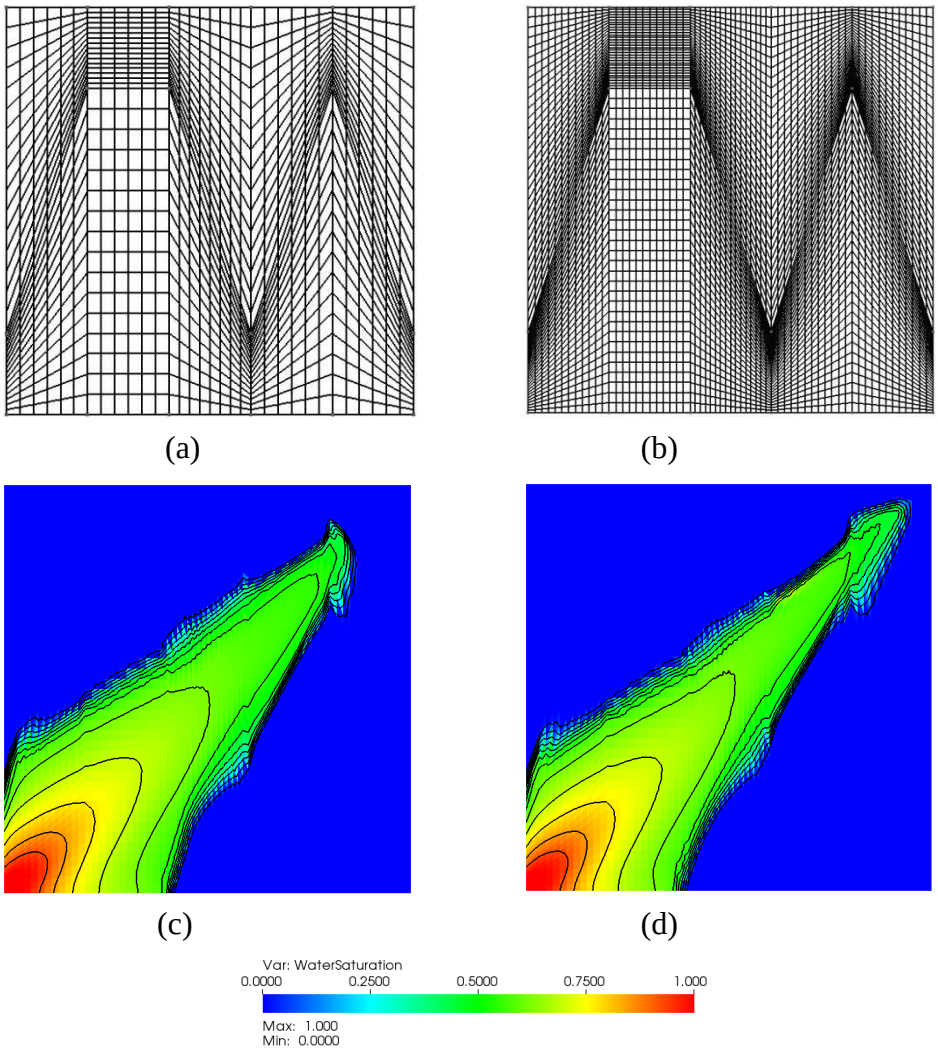

Figure 6. Water saturation field obtained for distorted mesh adapted from Hermeline (2007): (a) mesh with 32x32 subdivisions; (b) mesh with 64x64 subdivisions; (c) standard scheme with 2nd order of accuracy and MLPvk limiter (64x64 subdivisions); (d) M-TMU scheme with 2nd order of accuracy and MLPvk limiter (64x64 subdivisions).

Now, comparing each type of flow oriented scheme we can see that all TMU-type configurations (TMU and M-TMU) have presented better results than SMU-type results. Both TMU-type and SMU-type configurations have presented better results than that obtained with the standard schemes. Regarding the performance of the correction for distorted meshes, which leads to M-TMU and M-SMU approaches, we observe that for first order approximation there is no relevant gain whether M-TMU or TMU is used. When we compare M-SMU and SMU, we can see a slight gain, even for first order approximation. It occurs in both mesh refinements. It is interesting observe that both M-TMU and TMU with first order approximation produces oil flow rate curves practically matching to that obtained with higher order standard scheme. On the other hand, the influence of the correction for distorted meshes is substantial in higher order approximation schemes. Observing the curves in Fig. 7, we can perceive the M-TMU closer to the reference solution than the solution obtained with TMU. The same occurs for M-SMU compared to SMU. Moreover, the higher order M-SMU matches to higher order TMU.

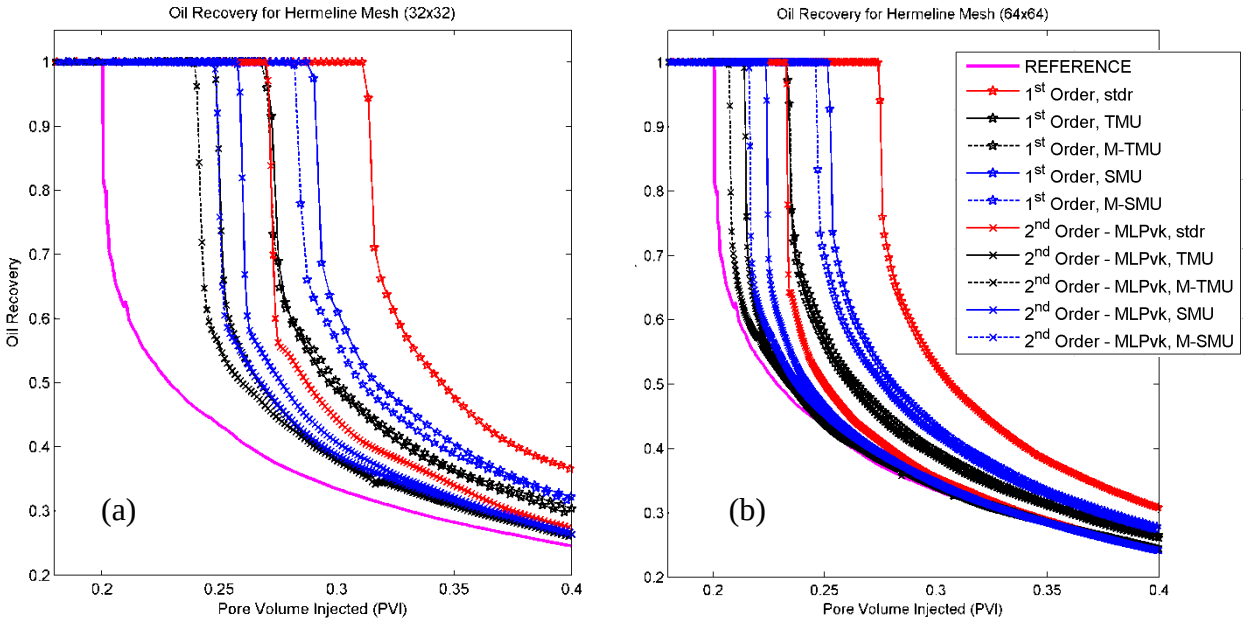

Figure 7. Oil flow rate curves for standard scheme (stdr), flow oriented scheme (TMU and SMU) and modified flow oriented scheme (M-TMU and M-SMU): (a) obtained in a 32x32 distorted mesh: (b) obtained in a 64x64 distorted mesh.

Again this performance is observed for both mesh refinements. In Fig. 7 we can see the performance of some configuration for the same time level. The improvement on the solution of the water saturation field, with respect to the diminishing of GOE is evident. It leads the breakthrough closer to that in reference solution.

5 CONCLUSIONS

In this paper we presented an alternative flow oriented scheme to solve two-phase flow in anisotropic petroleum reservoirs. This proposition has as main novelties the explicit computation of the multidimensional numerical fluxes on each half-surface, the introduction of an adaptive correction for the flow oriented scheme, according to the level of mesh distortion, and an efficient entropy fix, employed to enhance convergence and accuracy for the results. In this framework, low and higher orders of accuracy in space were performed, where, for higher order approximation, the MLP strategy was adopted due to its robustness and multidimensional character. The set of numerical procedures presented in this paper poses as advantageous when faced to another flow oriented-type schemes available in literature and with similar computation (Hurtado *et al*., 2007; Kozdon *et al*., 2011). In these last cases, the multidimensional numerical fluxes are implicitly calculated, with only first order of accuracy and without any entropy fix strategy. Some representative test cases were used in present paper to show the potential of the numerical procedures presented to handle problems involving adverse mobility ratio, highly anisotropic media and discretization with much distorted meshes.

We could observe, for a simple Buckley-Leverett problem, that the use of the Serna (2009) entropy fix enhances, in general, the convergence and accuracy of numerical solutions, predominantly obtained for second order of accuracy on space. The results obtained with

MLPvk as limiting strategy were the best ones. However, this entropy fix proposal was not capable to ensure that non-physical solutions could appear. Results obtained with the face-based limiter (van Albada) and with the traditional MLP limiter presented non-physical solutions near discontinuity and hence degradation on the convergence rate. In the comparison between the standard and the flow oriented schemes for solving an adverse mobility ratio problem with distorted mesh, it is clear that the flow oriented schemes diminishes substantially the GOE, compared to those results obtained with the standard approximation. This behavior was observed for both first and second order of accuracy. In addition, the schemes with correction of the multidimensionality according to the mesh distortion (M-TMU and M-SMU) produced results much more reliable than those obtained by the standard schemes (stdr) and even those obtained with conventional flow oriented schemes, TMU and SMU. This reveals that, in fact, the correction procedure is necessary, especially for higher order approximation, which, once again, produced the most reliable results.

ACKNOWLEDGEMENTS

The authors would like to thank the following Brazilian research agencies: Pernambuco State Foundation for Science and Technology (FACEPE), Brazilian National Counsel of Technological and Scientific Development (CNPq) and CENPES-PETROBRAS (SIGER-Petrobras Network on Simulation and Management of Petroleum Reservoirs).

REFERENCES

AZIZ, K. and SETTARI, A. 1979. Petroleum Reservoir Simulation Applied. Science Publishers Ltd., London, England.

BASTIAN, P. 2002. Higher order discontinuous Galerkin methods for flow and transport in porous media. In E. Bänsch, editor, Challenges in Scientific Computing – CISC 2002, volume 35 of Lecture Notes in Computational Science and Engineering, pages 1–22.

COLELLA, P. 1990. Multidimensional upwind methods for hyperbolic conservation laws *Journal of Computational Physics*; 87: 171–200.

CONTRERAS, F. R. L.; LYRA, P. R. M.; SOUZA, M. R. A.; CARVALHO, D. K. E. 2016. A cell-centered multipoint flux approximation method with a diamond stencil coupled with a higher order finite volume method for the simulation of oil–water displacements in heterogeneous and anisotropic petroleum reservoirs; *Computers & Fluids*, *127*, 1-16.

DELIS, A. I.; NIKOLOS, I. K. 2012. A Novel Multidimensional Solution Reconstruction and Edge-Based Limiting Procedure For Unstructured Cell-Centered Finite Volumes with Application to Shallow Water Dynamics. *Intern. Journ. Num. Methods Fluids*; 71: 584-633.

GAO, Z. M.; WU, J. M. 2010. A Linearity-Preserving Cell-Centered Scheme for the Heterogeneous and Anisotropic Diffusion Equations on General Meshes. *International Journal for Numerical Methods in Fluids*; 67: 2157-2183.

GOOCH, O. 1997. Quasi-ENO Schemes for Unstructured Meshes Based on Unlimited Data-Dependent Least-Squares Reconstruction, *J. of Computational Physics*; 133: 6–17.

HERMELINE, F. 2007. Approximation of 2-D and 3-D diffusion operators with variable full tensor coefficients on arbitrary meshes. *Computer meth. App. mech eng*; 196: 2497-2526.

HURTADO, F. S. V., MALISKA, A. F., da SILVA, A. F., CORDAZZO, J. 2007. A Quadrilateral Element-Based Finite-Volume Formulation for the Simulation of Complex Reservoir. In: SPE paper 107444-MS presented at the SPE Latin American and Caribbean Petroleum Engineering Conference held in Buenos Aires, Argentina; 15-18.

KOZDON, J. E; MALLISON, B. T.; GERITSEN, G. T. 2011. Multidimensional Upstream Weighting for Multiphase Transport in Porous Media. *Comp. Geoscience*; 15: 399–419.

LAMINE; EDWARDS, M. 2010. Multidimensional Convection Schemes for Flow in Porous Media on Structured and Unstructured Quadrilateral Grids. *J. C. A. Math*; 234: 2106-2117.

LAMINE, S.; EDWARDS, M. 2013. Higher Order Cell-Based Multidimensional Upwind Schemes for Flow in Porous Media on Unstructured Grids. *C. M. A. M. Eng.*; 259: 103-122.

LEVEQUE, R. J. 2002. Finite Volume Methods for Hyperbolic Problems. Cambridge University Press-London.

PARK, J. S.; YOON, S. H.; KIM, C. 2010. Multi-Dimensional Limiting Process for Hyperbolic Conservation Laws on Unstructured Grids. *J. of Comput. Physics*; 229: 788–812.

SCHNEIDER, G. E. e RAW, M. J. 1986. A Skewed, Positive Influence Coefficient Upwinding Procedure for Control-Volume-Based Finite-Element Convection-Diffusion Computation. *Numerical Heat Transfer*; 9: 1-26.

SERNA, S. 2009. A Characteristic-Based Nonconvex Entropy-Fix Upwind Scheme for the Ideal Magnetohydrodynamic Equations. *Journal of Computational Physics*; 228: 4232-4247.

SHU, C. W.; OSHER, S. 1989. Efficient Implementation Of Essentially Non-Oscillatory Shock-Capturing Schemes 2, *Journal of Computational Physics*; 83: 32–78.

SOUZA, M. 2015. Simulação Numérica de Escoamento Bifásico em Reservatórios de Petróleo Heterogêneos e Anisotrópicos Utilizando um Método de Volumes Finitos "Verdadeiramente" Multidimensional com Aproximação de Alta Ordem. Tese de doutorado. UFPE, Recife.

TRAN, D.; MASSON, C.; SMAÏLI, A. 2006. A stable second-order mass-weighted upwind scheme for unstructured meshes. *Int. journal for numerical methods in fluids*; 51: 749-771.

VAN ALBADA, G. D.; VAN LEER, B. ROBERTS Jr, W. W. 1982. A Comparative Study of Computational Methods in Cosmic gas Dynamics. *Astron. and Astrophysics*; 32: 76-84.

VAN LEER, B. 1979. Towards the ultimate conservative difference scheme V: A Second-order sequel to Godunov's method, *Journal of Computational Physics.*; 32: 101.

VENKATAKRISHNAN, V. 1995. Convergence to Steady-State Solutions of the Euler Equations on Unstruckred Grids with Limiters. *J. Computational Physics*. 118: 120-130.